

Semiconducting-to-Metallic Photoconductivity Crossover and Temperature-Dependent Drude Weight in Graphene

A. J. Frenzel,^{1,2} C. H. Lui,¹ Y. C. Shin,³ J. Kong,⁴ and N. Gedik^{1,*}

¹*Department of Physics, Massachusetts Institute of Technology, Cambridge, Massachusetts 02139, USA*

²*Department of Physics, Harvard University, Cambridge, Massachusetts 02138, USA*

³*Department of Materials Science and Engineering, Massachusetts Institute of Technology, Cambridge, Massachusetts 02139, USA*

⁴*Department of Electrical Engineering and Computer Science, Massachusetts Institute of Technology, Cambridge, Massachusetts 02139, USA*

(Received 14 March 2014; published 31 July 2014)

We investigate the transient photoconductivity of graphene at various gate-tuned carrier densities by optical-pump terahertz-probe spectroscopy. We demonstrate that graphene exhibits semiconducting positive photoconductivity near zero carrier density, which crosses over to metallic negative photoconductivity at high carrier density. These observations can be accounted for by the interplay between photoinduced changes of both the Drude weight and carrier scattering rate. Our findings provide a complete picture to explain the opposite photoconductivity behavior reported in (undoped) graphene grown epitaxially and (doped) graphene grown by chemical vapor deposition. Notably, we observe nonmonotonic fluence dependence of the photoconductivity at low carrier density. This behavior reveals the nonmonotonic temperature dependence of the Drude weight in graphene, a unique property of two-dimensional massless Dirac fermions.

DOI: [10.1103/PhysRevLett.113.056602](https://doi.org/10.1103/PhysRevLett.113.056602)

PACS numbers: 72.80.Vp, 72.40.+w, 73.40.Qv, 78.20.-e

Charge carriers in graphene mimic two-dimensional (2D) massless Dirac fermions with linear energy dispersion, resulting in unique optical and electronic properties [1]. They exhibit high mobility and strong interaction with electromagnetic radiation over a broad frequency range [2]. Interband transitions in graphene give rise to pronounced optical absorption in the midinfrared to visible spectral range, where the optical conductivity is close to a universal value $\sigma_0 = \pi e^2/2h$ [3]. Free-carrier intraband transitions, on the other hand, cause low-frequency absorption, which varies significantly with charge density and results in strong light extinction at high carrier density [4]. In addition to this density dependence, the massless Dirac particles in graphene are predicted to exhibit a distinctive nonmonotonic temperature dependence of the intraband absorption strength, or Drude weight, due to their linear dispersion [5,6]. This behavior contrasts with the temperature-independent Drude weight expected in conventional systems of massive particles with parabolic dispersion [7,8]. Although the unique behavior of the Drude weight in graphene has been considered theoretically, experimental signatures are still lacking.

The intrinsic properties of Drude absorption in graphene can be revealed by studying its dynamical response to photoexcitation. In particular, optical-pump terahertz-probe spectroscopy provides access to a wide transient temperature range via pulsed optical excitation, and allows measurement of the ac Drude conductivity by a time-delayed terahertz probe pulse [9]. This technique has been

applied to study transient photoconductivity (PC) in graphene, but conflicting results have been reported [9–15]. Positive PC was observed in epitaxial graphene on SiC (Ref. [15]), while negative PC was seen in graphene grown by chemical vapor deposition (CVD) [11–14]. It has been argued that the opposite behavior in these samples arises from their different charge densities. Here we study graphene samples with gate tunable carrier density to resolve these issues and further reveal the unique Drude response of massless Dirac fermions.

In this Letter, we present an investigation of the Drude absorption dynamics in graphene over a wide range of carrier density and temperature. Using optical-pump terahertz-probe spectroscopy, we drove the carriers to high transient temperature and probed the Drude absorption of the hot carriers as they relaxed to equilibrium. By adjusting the gate voltage, pump-probe delay, and excitation fluence, we were able to observe the change of Drude absorption over a broad range of carrier density and transient temperature. Near the charge neutrality point, our samples exhibited positive (semiconducting) ultrafast PC, due to thermal excitation of electron-hole pairs after photoexcitation. At high charge density, however, the samples exhibited negative (metallic) PC due to the decrease of both the Drude weight and the carrier scattering time at high transient temperature. The observed density-dependent PC provides a unifying framework for understanding previously reported positive PC in (undoped) epitaxial graphene and negative PC in (*p*-doped) CVD graphene.

Additionally, at low charge density, we observed unusual fluence dependence of the terahertz Drude response, where the PC first decreased and then increased as the pump fluence increased. This is consistent with the behavior expected from the nonmonotonic temperature dependence of the Drude weight in graphene. By using the Drude model with an estimated temporal evolution of the hot carrier temperature, we were able to reproduce our main observations.

A key advance in our experiment is the fabrication of large-area gated graphene devices without a terahertz PC response from the substrate [Fig. 1(a)]. This is not possible with commonly used SiO_2/Si substrates, which produce a large background signal in optical-pump terahertz-probe experiments [16]. We used z -cut crystalline quartz substrates and deposited 35-nm indium tin oxide (ITO) and 400-nm parylene-C thin films as the back-gate electrode and dielectric, respectively. We experimentally confirmed that the back-gate structure had negligible pump-probe response (see the Supplemental Material [17]). High-quality single-layer CVD graphene sheets [28] were transferred onto our back-gate substrates. Graphite-paint source and drain electrodes were attached to graphene with a separation of ~ 5 mm. The devices exhibited excellent bipolar gating behavior with low unintentional doping [Fig. 1(b); gate voltage $V_g = 3$ V $\equiv V_{\text{CN}}$ at charge neutrality (CN), corresponding to unintentional hole doping

$p = 1.7 \times 10^{11}$ cm^{-2} , estimated from our device capacitance].

The graphene devices, investigated at room temperature in high vacuum ($P < 10^{-5}$ Torr), were photoexcited with 100 fs laser pulses at 1.55 eV photon energy generated using a 5 kHz amplified Ti:sapphire laser system. The transient PC was probed by measuring the complex transmission coefficient of time-delayed picosecond terahertz pulses (photon energy 2–10 meV) with controllable time delay τ [Fig. 1(a)]. In these measurements, the local detection time of the picosecond terahertz pulse was synchronized with the pump pulse such that the whole terahertz waveform experienced the same time delay after photoexcitation [29]. To reduce experimental errors due to laser drift, we simultaneously measured the transmitted terahertz electric field waveform $E_0(t)$ without optical excitation and the optical-pump-induced change of the field $\Delta E_\tau(t)$ via electro-optic sampling using a data acquisition card [16,17,30]. The resulting ratio $-\Delta E_\tau/E_0$ (referred to as “differential field”) approximately represents the PC, $\Delta\sigma_{\tau,1}$ (Refs. [9–12,17]).

Pump-probe measurements with incident pump fluence $\mathcal{F} = 10$ $\mu\text{J}/\text{cm}^2$ and pump-probe delay $\tau = 1.5$ ps reveal that the sign of the PC changes from positive near charge neutrality to negative at moderate carrier density [Fig. 2]. The measured $\Delta E_\tau(t)$ near charge neutrality ($V_g = V_{\text{CN}} + 2$ V) is opposite in sign to $E_0(t)$ for all t , reflecting photoenhanced absorption [Fig. 2(a)]. The extracted PC spectrum $\Delta\sigma_\tau(\omega) = \Delta\sigma_{\tau,1} + i\Delta\sigma_{\tau,2}$, calculated with the device geometry taken into account (see the Supplemental Material [17]), shows a positive real part [Fig. 2(b)]. In sharp contrast, $\Delta E_\tau(t)$ has the same form and sign as $E_0(t)$ when $V_g = V_{\text{CN}} + 52$ V ($n \approx 3 \times 10^{12}$ cm^{-2}), indicating a photoinduced decrease in absorption [Fig. 2(d)]. As expected, the real part of the PC, $\Delta\sigma_{\tau,1}$, is negative in this case [Fig. 2(e)].

To further investigate the mechanism driving the observed PC sign change, we measured the temporal (τ) dynamics of $\Delta\sigma_{\tau,1}$ at various carrier densities. Figure 3(a) displays the ratio $-\Delta E_\tau(t)/E_0(t)$ as a function of τ at fixed $t = 0$ [Figs. 2(a) and 2(d)] for gate voltages between -48 and $+2$ V from V_{CN} (incident fluence $\mathcal{F} = 10$ $\mu\text{J}/\text{cm}^2$). The dynamics exhibits a relaxation time of ~ 2 ps, with no systematic dependence on carrier density. From these dynamical data, we evaluated the differential field averaged over τ , $\langle -\Delta E_\tau/E_0 \rangle_\tau$, as a function of gate voltage [Fig. 3(c)]. The result demonstrates that the overall PC signal changes from positive at charge neutrality to negative at moderate charge density for both electron and hole sides, consistent with dc measurements [31]. Similar results were observed at different fluences (see, for example, results for $\mathcal{F} = 3$ $\mu\text{J}/\text{cm}^2$ in the Supplemental Material [17]).

The above observations can be qualitatively understood by considering the interplay between photoinduced changes of carrier population and scattering rate. Photoexcited carriers in graphene are known to thermalize within a few tens of femtoseconds [32]. With the > 100 fs resolution in

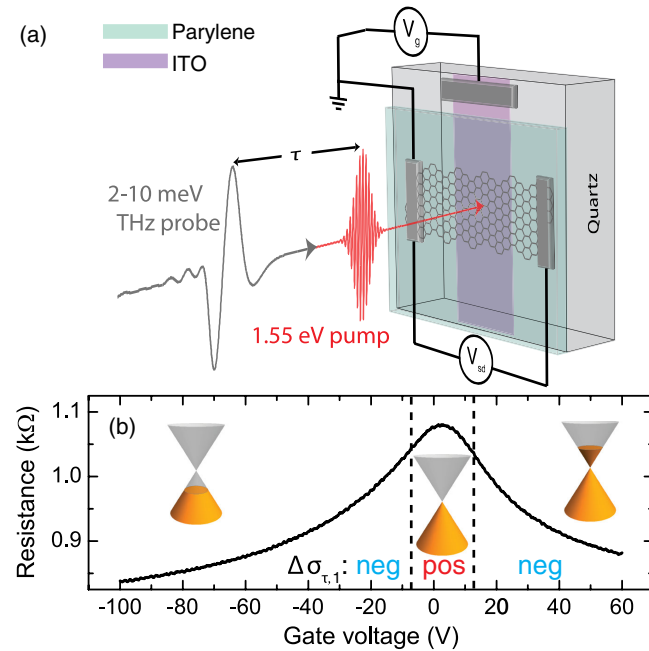


FIG. 1 (color online). (a) Schematic of transparent graphene device geometry and experimental method described in the text. (b) Two-terminal resistance of our device as a function of back-gate voltage V_g . The charge neutrality point, corresponding to maximum resistance, is at $V_g = V_{\text{CN}} = 3$ V. Voltage ranges of positive and negative photoconductivity ($\Delta\sigma_{\tau,1}$) observed in our experiment are separated by dashed vertical lines.

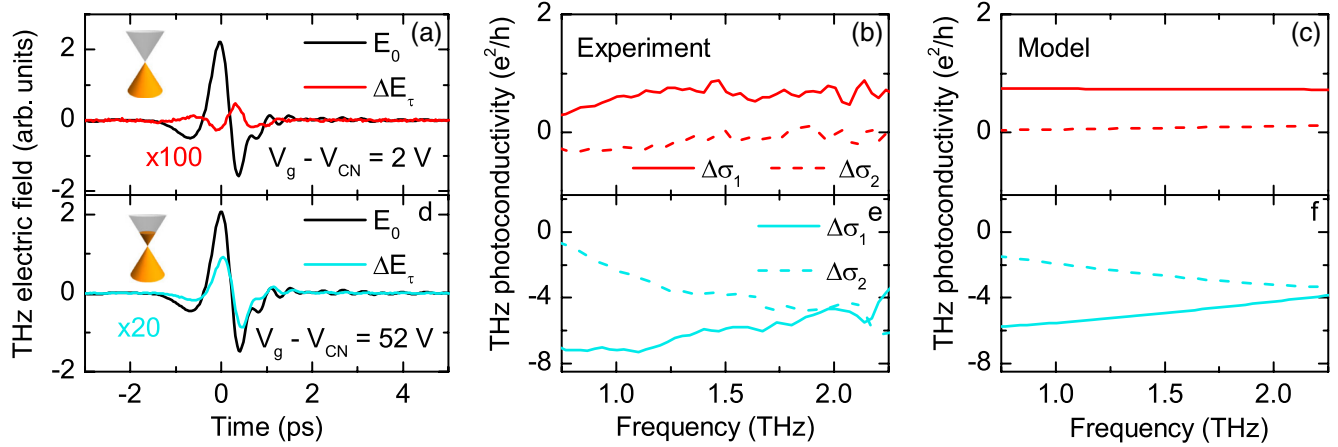


FIG. 2 (color online). (a) Measured terahertz electric field waveform transmitted through the sample in equilibrium (black line) and pump-induced change in transmitted terahertz electric field (red line) at $\tau = 1.5$ ps. Measurements were performed at room temperature in vacuum with the carrier density set near charge neutrality ($V_g = V_{CN} + 2$ V) and incident pump fluence $\mathcal{F} = 10 \mu\text{J}/\text{cm}^2$. (b) Real ($\Delta\sigma_1$, solid line) and imaginary ($\Delta\sigma_2$, dashed line) parts of the transient terahertz PC extracted from the data in (a). (c) Theoretical simulation of the PC spectra under the same conditions as (a),(b) using the Drude model described in the text. (d)–(f) Experimental data and simulation as in (a)–(c), but at gate voltage +52 V from the charge neutrality point (electron density $n \approx 3 \times 10^{12} \text{ cm}^{-2}$).

our experiment, the carriers can be well described by a thermal distribution at temperature T_e for all pump-probe delay times τ . For graphene near the charge neutrality point, an increase of carrier temperature promotes the free-carrier population and thus enhances absorption. This behavior

mimics that observed in epitaxial graphene [15] and other semiconductors [9,29], where optically generated electron-hole pairs increase the infrared absorption. For graphene with high carrier density, laser-induced carrier heating only modifies the carrier distribution near the Fermi level, without changing the total carrier density. The carrier scattering rate, however, increases due to an enlarged phase space and the presence of hot optical phonons [33]. This causes a reduction of free-carrier absorption, a behavior analogous to that in metals and observed in *p*-doped CVD graphene [11–14].

For a more thorough understanding of the density-dependent PC dynamics, we consider a Drude model for free carrier conductivity in graphene [4,6,11,12,15],

$$\sigma(\omega) = \frac{D}{\pi(\Gamma - i\omega)}. \quad (1)$$

Here, Γ is the transport scattering rate and D is the Drude weight, which quantifies the oscillator strength of free-carrier absorption. In a metal or semiconductor with parabolic dispersion, $D = \pi n e^2 / m$, independent of temperature [8,17]. In graphene, a 2D system with linear dispersion, however, D exhibits a distinctive carrier temperature dependence [5,6,17,34],

$$D(T_e) = \frac{2e^2}{\hbar^2} k_B T_e \ln \left[2 \cosh \left(\frac{\mu(T_e)}{2k_B T_e} \right) \right]. \quad (2)$$

This relation predicts that, in intrinsic graphene, $D(T_e)$ increases linearly with temperature when $k_B T_e \gg \epsilon_F$, and approaches $(e^2/\hbar^2)\mu \propto \sqrt{|n|}$ for electronic temperatures $k_B T_e \ll \epsilon_F$. For graphene samples on substrates, charge inhomogeneity and disorder smear out intrinsic behavior near the Dirac point [35]. We include these effects by using a phenomenologically broadened chemical potential

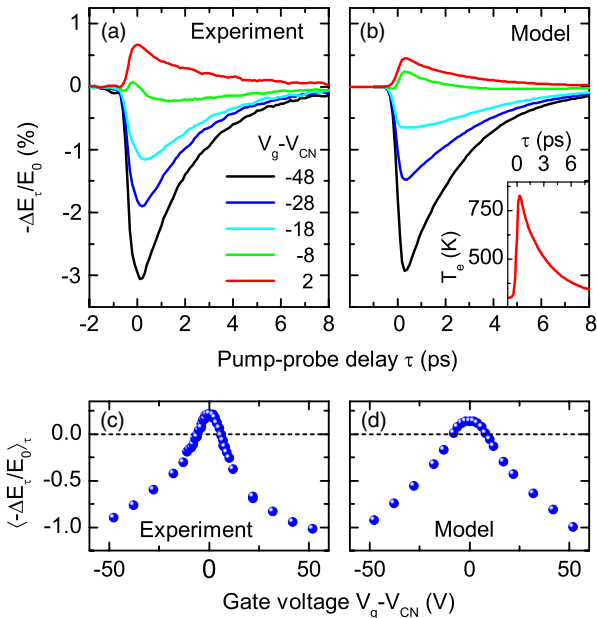


FIG. 3 (color online). (a) Measured temporal evolution of the negative change in transmitted field (proportional to the differential conductivity), measured at the peak of the signal in Figs. 2(a) and 2(d), at different gate voltages. Measurements were performed at room temperature in vacuum with incident fluence $\mathcal{F} = 10 \mu\text{J}/\text{cm}^2$. (b) Theoretical simulation of the terahertz dynamics in (a), calculated using the model described in the text. Inset shows the estimated temperature profile used to model the data. (c) Mean of $-\Delta E(t=0)_\tau / E_0(t=0)$ from $\tau = -1$ to 8 ps, as a function of gate voltage. (d) Simulation of the data in (c).

$\mu \rightarrow \sqrt{\mu^4 + \Delta^4}$, with $\Delta = 80$ meV, a reasonable value for our samples [17,36].

The other parameter in the Drude model, the scattering rate Γ , depends on the chemical potential μ , the carrier temperature T_e , the phonon temperature T_{ph} , and the specific scattering mechanisms [37]. In our samples, we expect charged impurities and hot optical phonons to dominate scattering [17,33,37,38]. To facilitate our calculations, we consider a contribution $\Gamma_C \propto |\mu|^{-1}$ due to Coulomb impurity scattering [35] and the expression given in Ref. [38] for scattering with intrinsic optical phonons, assuming that $T_{\text{ph}} = T_e$ [Refs. [10,32]; Fig. 4(b)]. We neglect the unknown coupling of carriers to surface phonons in the parylene-C dielectric [31,37].

We used $D(T_e)$ and $\Gamma(T_e, T_{\text{ph}})$ as estimated above to calculate the temperature- and density-dependent change of conductivity for our experimental conditions, $\Delta\sigma_1(T_e) = \sigma_1(T_e) - \sigma_1(300 \text{ K})$, at a representative frequency $\omega/2\pi = 1$ THz. The result [Fig. 4(c)] shows that $\Delta\sigma_1(T_e)$ is positive (red area) near charge neutrality ($V_g < 5$ V), but becomes negative (blue area) at high carrier density ($V_g > 15$ V), as anticipated from the qualitative discussion above.

To simulate the transient PC dynamics, we also considered the temporal (τ) evolution of the carrier temperature after photoexcitation. Such hot carrier dynamics have been discussed extensively in the literature. We therefore

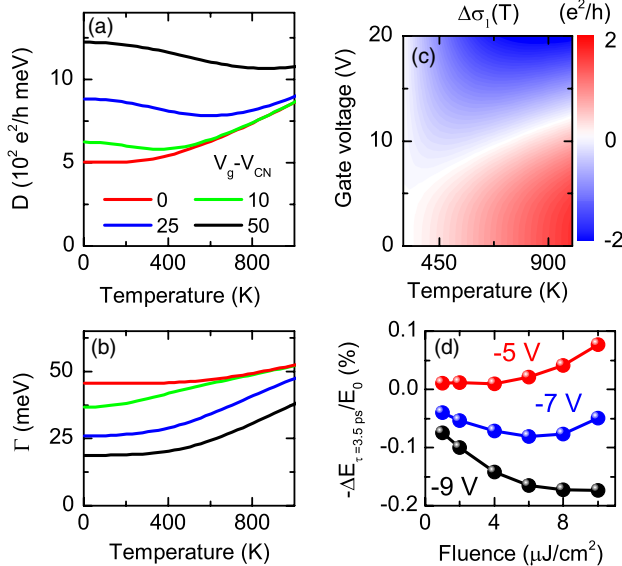


FIG. 4 (color online). (a) Temperature-dependent Drude weight [Eq. (2)] at different gate voltages. Saturation at low temperature is due to charge disorder. (b) Estimated temperature dependence of the scattering rate at different gate voltages. (c) Calculated change in conductivity $\Delta\sigma_1(T)$ at $\omega/2\pi = 1$ THz, for different carrier densities and temperatures, relative to its value at $T = 300$ K. Temperature dependence of both the Drude weight and scattering rate were taken into account. (d) Fluence dependence of PC at fixed pump-probe delay $\tau = 3.5$ ps showing the nonmonotonic behavior expected from our model.

estimated the transient temperature profile from previous publications [32,33,39] and simulated the temporal PC dynamics. In particular, we assumed a biexponential decay with time constants $\tau_1 = 0.3$ ps and $\tau_2 = 3.1$ ps and a 200 fs rise time [Refs. [33,39]; see inset of Fig. 3(b)]. The maximum estimated temperature was ~ 800 K for incident fluence $10 \mu\text{J}/\text{cm}^2$. Based on this temperature profile, we calculated $\Delta\sigma_\tau(\omega)$ [Figs. 2(c) and 2(f)] and $-\Delta E_\tau/E_0$ [Figs. 3(b) and 3(d)]. Our simulations, though based on a simple model, were found to reproduce all the main features of our observations.

An essential aspect of our model is the distinctive Drude weight of graphene with nonmonotonic temperature dependence [Eq. (2) and Fig. 4(a)]. Specifically, for finite carrier density, $D(T_e)$ first decreases to a minimum value as T_e increases, then increases linearly with T_e for temperatures much greater than ε_F [Fig. 4(a); Refs. [5,17]]. Simulations performed without considering this temperature dependence yielded results qualitatively different from the experimental data (see Fig. S7 of the Supplemental Material [17]). In order to reveal this unique Drude behavior of graphene more directly, we examined the fluence dependence of $-\Delta E_\tau/E_0$ in the PC crossover regime [Fig. 4(d)]. Since T_e increases monotonically with excitation fluence [32,33], any nonmonotonicity of $D(T_e)$ should also manifest in its fluence dependence. This phenomenon was indeed observed in our experiment [Fig. 4(d)]. At a representative $\tau = 3.5$ ps near the PC crossover ($V_g = -7$ V), $-\Delta E_{3.5 \text{ ps}}/E_0$ was found to first decrease and then increase with increasing fluence. This nonmonotonic behavior gradually weakens as the density moves away from the crossover (see, e.g., $V_g = -5$ and -9 V in Fig. 4(d)). This peculiar fluence dependence was observed for all $\tau = 1$ –8 ps. We also observed independent evidence for the nonmonotonic $D(T_e)$ in the temporal PC dynamics at the crossover, where the PC sign flips multiple times as the carriers are heated up by the pump pulse and subsequently cool (see the Supplemental Material [17] for details).

The observed nonmonotonic temperature dependence of the Drude weight can be understood by considering conservation of spectral weight of optical transitions [4,6,40]. Optical absorption in graphene consists of two contributions: high-energy interband absorption and low-energy intraband absorption. Interband absorption in graphene with finite charge density shows an onset at photon energy $\hbar\omega = 2|\mu|$ due to Pauli blocking [3,4,6]. When carriers are heated to moderate temperatures $k_B T_e \ll \varepsilon_F$, $\mu(T_e)$ decreases due to particle conservation [8]. The corresponding decrease of onset energy for interband absorption increases the interband spectral weight. To conserve total spectral weight, the intraband absorption must decrease. When carrier temperatures become comparable to ε_F , however, interband transitions are Pauli blocked by thermally excited carriers, reducing the spectral weight. This increases the intraband spectral weight, as has been observed in graphite [40]. This unique behavior

originates from the distinctive linear dispersion of 2D massless Dirac fermions in graphene, and is absent in conventional materials with parabolic dispersion.

In conclusion, we have studied the temperature- and density-dependent Drude conductivity in graphene through its dynamical response to pulsed photoexcitation. We demonstrated that the transient photoconductivity of graphene can be tuned continuously from semiconducting to metallic by varying the Fermi level from the charge neutrality point to either the electron or hole side. Our results resolve the controversy between previous experiments, which observed positive photoconductivity in epitaxial graphene and negative photoconductivity in CVD graphene. By detailed simulation based on the Drude model, we found that photoinduced changes of both the Drude weight and carrier scattering rate play important roles in the terahertz photoconductivity dynamics.

We acknowledge J. C. W. Song and O. Khatib for helpful discussions; V. Fatemi, J. D. Sanchez-Yamagishi, and M. A. Smith for assistance with device fabrication; and D. V. Pilon for assistance with experiments. This work was supported by the U.S. Department of Energy Office of Basic Energy Sciences Grant No. DE-SC0006423 (sample fabrication, experimental setup, and data acquisition) and STC Center for Integrated Quantum Materials, NSF Grant No. DMR-1231319 (data analysis). A. J. F. acknowledges support from NSF GRFP. This work also made use of Harvard's Center for Nanoscale Systems (CNS), supported by the National Science Foundation under Grant No. ECS-0335765, and the MIT Microsystems Technology Laboratory (MTL).

Note added.—Recently we became aware of similar work by another group [41].

*gedik@mit.edu

- [1] A. H. Castro Neto, F. Guinea, N. M. R. Peres, K. S. Novoselov, and A. K. Geim, *Rev. Mod. Phys.* **81**, 109 (2009); S. Das Sarma, S. Adam, E. H. Hwang, and E. Rossi, *Rev. Mod. Phys.* **83**, 407 (2011).
- [2] K. F. Mak, L. Ju, F. Wang, and T. F. Heinz, *Solid State Commun.* **152**, 1341 (2012).
- [3] K. F. Mak, M. Y. Sfeir, Y. Wu, C. H. Lui, J. A. Misewich, and T. F. Heinz, *Phys. Rev. Lett.* **101**, 196405 (2008); Z. Q. Li, E. A. Henriksen, Z. Jiang, Z. Hao, M. C. Martin, P. Kim, H. L. Stormer, and D. N. Basov, *Nat. Phys.* **4**, 532 (2008); F. Wang, Y. Zhang, C. Tian, C. Girit, A. Zettl, M. Crommie, and Y. R. Shen, *Science* **320**, 206 (2008).
- [4] J. Horng, C.-F. Chen, B. Geng, C. Girit, Y. Zhang, Z. Hao, H. A. Bechtel, M. Martin, A. Zettl, M. F. Crommie, Y. R. Shen, and F. Wang, *Phys. Rev. B* **83**, 165113 (2011); L. Ren, Q. Zhang, J. Yao, Z. Sun, R. Kaneko, Z. Yan, S. Nanot, Z. Jin, I. Kawayama, M. Tonouchi, J. M. Tour, and J. Kono, *Nano Lett.* **12**, 3711 (2012).
- [5] M. Müller, M. Bräuninger, and B. Trauzettel, *Phys. Rev. Lett.* **103**, 196801 (2009).

- [6] V. P. Gusynin, S. G. Sharapov, and J. P. Carbotte, *New J. Phys.* **11**, 095013 (2009).
- [7] V. P. Gusynin, S. G. Sharapov, and J. P. Carbotte, *Phys. Rev. B* **75**, 165407 (2007).
- [8] N. W. Ashcroft and N. D. Mermin, *Solid State Physics* (Brooks-Cole, Belmont, MA, 1976).
- [9] R. Ulbricht, E. Hendry, J. Shan, T. F. Heinz, and M. Bonn, *Rev. Mod. Phys.* **83**, 543 (2011).
- [10] T. Kampfrath, L. Perfetti, F. Schapper, C. Frischkorn, and M. Wolf, *Phys. Rev. Lett.* **95**, 187403 (2005).
- [11] G. Jnawali, Y. Rao, H. Yan, and T. F. Heinz, *Nano Lett.* **13**, 524 (2013).
- [12] A. J. Frenzel, C. H. Lui, W. Fang, N. L. Nair, P. K. Herring, P. Jarillo-Herrero, J. Kong, and N. Gedik, *Appl. Phys. Lett.* **102**, 113111 (2013).
- [13] C. J. Docherty, C.-T. Lin, H. J. Joyce, R. J. Nicholas, L. M. Herz, L.-J. Li, and M. B. Johnston, *Nat. Commun.* **3**, 1228 (2012).
- [14] K. J. Tielrooij, J. C. W. Song, S. A. Jensen, A. Centeno, A. Pesquera, A. Zurutuza Elorza, M. Bonn, L. S. Levitov, and F. H. L. Koppens, *Nat. Phys.* **9**, 248 (2013).
- [15] H. Choi, F. Borondics, D. A. Siegel, S. Y. Zhou, M. C. Martin, A. Lanzara, and R. A. Kaindl, *Appl. Phys. Lett.* **94**, 172102 (2009); J. H. Strait, H. Wang, S. Shivaraman, V. Shields, M. Spencer, and F. Rana, *Nano Lett.* **11**, 4902 (2011); S. Winnerl, M. Orlita, P. Plochocka, P. Kossacki, M. Potemski, T. Winzer, E. Malic, A. Knorr, M. Sprinkle, C. Berger, W. A. de Heer, H. Schneider, and M. Helm, *Phys. Rev. Lett.* **107**, 237401 (2011); J. Kim, S. C. Lim, S. J. Chae, I. Maeng, Y. Choi, S. Cha, Y. H. Lee, and H. Choi, *Sci. Rep.* **3**, 02663 (2013).
- [16] K. Iwaszczuk, D. G. Cooke, M. Fujiwara, H. Hashimoto, and P. U. Jepsen, *Opt. Express* **17**, 21969 (2009).
- [17] See Supplemental Material at <http://link.aps.org/supplemental/10.1103/PhysRevLett.113.056602>, which includes Refs. [18-27].
- [18] A. Kahouli, A. Sylvestre, L. Ortega, F. Jomni, B. Yangui, M. Maillard, B. Berge, J.-C. Robert, and J. Legrand, *Appl. Phys. Lett.* **94**, 152901 (2009).
- [19] R. D. Averitt, G. Rodriguez, J. L. W. Siders, S. A. Trugman, and A. J. Taylor, *J. Opt. Soc. Am. B* **17**, 327 (2000).
- [20] L. Duvillaret, F. Garet, and J.-L. Coutaz, *IEEE J. Sel. Top. Quantum Electron.* **2**, 739 (1996).
- [21] M. C. Nuss and J. Orenstein, in *Millimeter and Submillimeter Wave Spectroscopy of Solids*, edited by G. Grüner (Springer, Berlin, 1998) Chap. 2, pp. 7–50.
- [22] X. Liu, S. MacNaughton, D. B. Shrekenhamer, H. Tao, S. Selvarasah, A. Totachawattana, R. D. Averitt, M. R. Dokmeci, S. Sonkusale, and W. J. Padilla, *Appl. Phys. Lett.* **96**, 011906 (2010).
- [23] J.-H. Chen, C. Jang, S. Xiao, M. Ishigami, and M. S. Fuhrer, *Nat. Nanotechnol.* **3**, 206 (2008).
- [24] T. Stauber, N. M. R. Peres, and F. Guinea, *Phys. Rev. B* **76**, 205423 (2007).
- [25] K. He, L. Zhao, J. Shan, K. F. Mak, N. Petron, J. Hone, T. F. Heinz, and G. L. Carr, *Bull. Am. Phys. Soc.* **T5**, 8 (2013).
- [26] C. Larsen, D. G. Cooke, and P. U. Jepsen, *J. Opt. Soc. Am. B* **28**, 1308 (2011).
- [27] T. Ando, *J. Phys. Soc. Jpn.* **75**, 074716 (2006).
- [28] X. Li, W. Cai, J. An, S. Kim, J. Nah, D. Yang, R. Piner, A. Velamakanni, I. Jung, E. Tutuc, S. K. Banerjee, L. Colombo, and R. S. Ruoff, *Science* **324**, 1312 (2009).

- [29] M. C. Beard, G. M. Turner, and C. A. Schmuttenmaer, *Phys. Rev. B* **62**, 15764 (2000).
- [30] C. A. Werley, S. M. Teo, and K. A. Nelson, *Rev. Sci. Instrum.* **82**, 123108 (2011).
- [31] M. Freitag, T. Low, F. Xia, and P. Avouris, *Nat. Photonics* **7**, 53 (2012).
- [32] C. H. Lui, K. F. Mak, J. Shan, and T. F. Heinz, *Phys. Rev. Lett.* **105**, 127404 (2010); M. Breusing, S. Kuehn, T. Winzer, E. Malić, F. Milde, N. Severin, J. P. Rabe, C. Ropers, A. Knorr, and T. Elsaesser, *Phys. Rev. B* **83**, 153410 (2011); D. Brida, A. Tomadin, C. Manzoni, Y. J. Kim, A. Lombardo, S. Milana, R. R. Nair, K. S. Novoselov, A. C. Ferrari, G. Cerullo, and M. Polini, *Nat. Commun.* **4**, 1987 (2013); J. C. Johannsen, S. Ulstrup, F. Cilento, A. Crepaldi, M. Zacchigna, C. Cacho, I. C. Edmond Turcu, E. Springate, F. Fromm, C. Raidel, T. Seyller, F. Parmigiani, M. Grioni, and P. Hofmann, *Phys. Rev. Lett.* **111**, 027403 (2013); I. Gierz, J. C. Petersen, M. Mitrano, C. Cacho, I. C. E. Turcu, E. Springate, A. Stöhr, A. Köhler, U. Starke, and A. Cavalleri, *Nat. Mater.* **12**, 1119 (2013).
- [33] L. M. Malard, K. F. Mak, A. H. Castro Neto, N. M. R. Peres, and T. F. Heinz, *New J. Phys.* **15**, 015009 (2013).
- [34] M. Wagner, Z. Fei, A. S. McLeod, A. S. Rodin, W. Bao, E. G. Iwinski, Z. Zhao, M. Goldflam, M. Liu, G. Dominguez, M. Thiemens, M. M. Fogler, A. H. Castro Neto, C. N. Lau, S. Amarie, F. Keilmann, and D. N. Basov, *Nano Lett.* **14**, 894 (2014).
- [35] S. Adam, E. H. Hwang, V. M. Galitski, and S. Das Sarma, *Proc. Natl. Acad. Sci. U.S.A.* **104**, 18392 (2007).
- [36] S. Kim, J. Nah, I. Jo, D. Shahrjerdi, L. Colombo, Z. Yao, E. Tutuc, and S. K. Banerjee, *Appl. Phys. Lett.* **94**, 062107 (2009).
- [37] E. H. Hwang and S. Das Sarma, *Phys. Rev. B* **77**, 115449 (2008); S. Fratini and F. Guinea, *ibid.* **77**, 195415 (2008); E. H. Hwang and S. Das Sarma, *ibid.* **79**, 165404 (2009).
- [38] V. Perebeinos and P. Avouris, *Phys. Rev. B* **81**, 195442 (2010).
- [39] M. W. Graham, S.-F. Shi, Z. Wang, D. C. Ralph, J. Park, and P. L. McEuen, *Nano Lett.* **13**, 5497 (2013).
- [40] A. B. Kuzmenko, E. van Heumen, F. Carbone, and D. van der Marel, *Phys. Rev. Lett.* **100**, 117401 (2008).
- [41] S.-F. Shi, T.-T. Tang, B. Zeng, L. Ju, Q. Zhou, A. Zettl, and F. Wang, *Nano Lett.* **14**, 1578 (2014).